Cell Tissue Res (1999) 296:307–321

REGULAR ARTICLE

John E. Rash · Thomas Yasumura

Direct immunogold labeling of connexins and aquaporin-4 in freeze-fracture replicas of liver, brain, and spinal cord: factors limiting quantitative analysis

Received: 2 September 1998 / Accepted: 24 November 1998

Abstract Direct immunogold labeling and histological mapping of membrane proteins is demonstrated in Lexan-stabilized SDS-washed freeze-fracture replicas of complex tissues. Using rat brain and spinal cord as primary model systems and liver as a "control" tissue to identify preparation and labeling artifacts, we demonstrate the presence of connexin43 in freeze-fractured gap junctions of identified and mapped astrocytes and ependymocytes, and confirm the presence of connexin32 in freeze-fractured gap junctions in liver. In addition, the simultaneous double-labeling of dissimilar proteins (connexin43 and aquaporin-4) is demonstrated in gap junctions and square arrays, respectively, in the plasma membranes of astrocytes and ependymocytes. Finally, double-side shadowing and conventional staining methods are used to reveal the extent of biological material present at the time of labeling and to investigate the dynamics of membrane solubilization, the primary artifacts that occur during labeling, and several factors limiting quantitative analysis.

Key words Freeze fracture · Immunogold labeling · Connexins · Aquaporin-4 · Brain · Spinal cord

This work was supported by NIH grant NS-31027, and previously, by grants GM 39503 and NS-15991.

J. E. Rash (✉) · T. Yasumura
Department of Anatomy and Neurobiology,
Colorado State University, Fort Collins, CO 80523, USA
e-mail: jrash@cvmbs.colostate.edu;
Tel.: +1 970 491 5606; Fax: +1 970 491 7907

J. E. Rash
Program in Molecular, Cellular and Integrative Neurosciences,
Colorado State University, Fort Collins, CO 80523, USA

J. E. Rash
Program in Cell and Molecular Biology,
Colorado State University, Fort Collins, CO 80523, USA

Introduction

The simultaneous subcellular localization and biochemical identification of membrane proteins has been a major goal of freeze-fracture since the number and variety of intramembrane particles (IMPs) was correlated with the diverse enzymatic and functional states of biological membranes (Branton 1971; Singer and Nicolson 1972). Initially, it was assumed that IMPs could not be labeled directly, because no membrane proteins or other biological molecules remained after the replicas were cleaned for viewing by transmission electron microscopy (TEM). However, in the late 1970s and early 1980s, several useful but tedious methods for the labeling and viewing of membrane proteins were introduced (for a review, see Severs 1989). These included freeze-fracture autoradiography (Fisher and Branton 1976; Rash et al. 1981), sectioned-labeled replica methods (Rash et al. 1978, 1980; Pinto da Silva et al. 1981a), whole-mount viewing of labeled ultrathin samples (Pinto da Silva et al. 1981a, b; Andersson Forsman and Pinto da Silva 1988), and "fracture-flip" methods (Andersson Forsman and Pinto da Silva 1988).

In 1995, Fujimoto introduced a new approach for direct immunogold labeling of clustered or cross-linked membrane proteins in detergent-cleaned freeze-fracture replicas (Fujimoto 1995, 1997). He demonstrated that washes in SDS detergent preferentially removed almost all cellular components except those in direct (i.e., "adsorptive") contact with the replica film. With a simple homogeneous tissue model (i.e., liver), Fujimoto demonstrated direct immunogold labeling of residual gap-junction and tight-junction proteins by using antibodies to connexin32 (Cx32), occludin, and ZO-1 (Fujimoto 1995, 1997). However, the initial SDS-fracture label method (SDS-FRL) was not useful for identifying membrane proteins in complex tissues, such as brain or spinal cord, because of several limitations. Foremost, the original methods required strong agitation of fragile replicas in SDS detergent; this resulted in severe fragmentation of replicas. The consequent loss of histological orientation in the replica fragments prevented any meaningful corre-

lation of labeled molecules with individual mapped cells in complex tissue. Second, substantial patience and dexterity was required to collect, unfold, and mount the 0.1-mm^2 replica fragments that remained after strong agitation in SDS detergent. Third, the nature of the SDS-solubilization process was not investigated, nor was the conjecture tested that it was the carbon component of the platinum/carbon (Pt/C) replica film (rather than the accompanying platinum atoms) that was responsible for protein adsorptivity and/or resistance to detergent washing (Fujimoto 1995).

To overcome the limitations created by fragmentation of complex tissues, we have modified the SDS-washing procedure to make it compatible with "grid-mapped" freeze-fracture (Rash et al. 1995, 1996). We have also investigated the proposed role of carbon films in the differential adsorption of membrane proteins. We now describe modified methods for freeze-fracture immunocytochemistry that permit the simultaneous in situ identification, histological mapping, and subcellular localization of membrane proteins in complex tissues and the simultaneous localization of two or more unlike proteins to distinctive arrays of IMPs in histologically mapped and cytologically identified cells in rat brain and spinal cord. We have also characterized the primary artifacts and anomalies of immunogold labeling of SDS-washed tissues (i.e., "false positives," "false negatives," and "cryptic" labeling). Furthermore, we describe ultrastructural changes in membranes that occur during the SDS-cleaning process and provide supporting evidence that carbon atoms provide the primary source of adsorption of membrane proteins to the replica film. The combination of SDS-FRL and grid-mapped freeze-fracture thus now allows the biochemical identification and ultrastructural mapping of membrane proteins in a wide variety of complex tissues.

Materials and methods

Sources of tissue

Sprague-Dawley rats (2 males, 8 females; 200–500 g) were anesthetized (ketamine 90 mg/kg; xylazine 8 mg/kg) and fixed for 10 min via transcardiac perfusion with 1% formaldehyde (glutaraldehyde-fixed tissues cannot be cleaned with SDS detergent) in 0.15 M Sörensen's phosphate buffer (SPB) as described in Hudson et al. (1981). All experiments were conducted according to the "Principles of laboratory animal care" (NIH publication no. 86–23, revised 1985).

Grid-mapped freeze-fracture

Samples of brain, spinal cord, and liver were cut into 100-µm-thick slices (Fig. 1, Step 1) by using a refrigerated Lancer 1000 vibratome operated at 4°C. Tissue slices were infiltrated with 30%

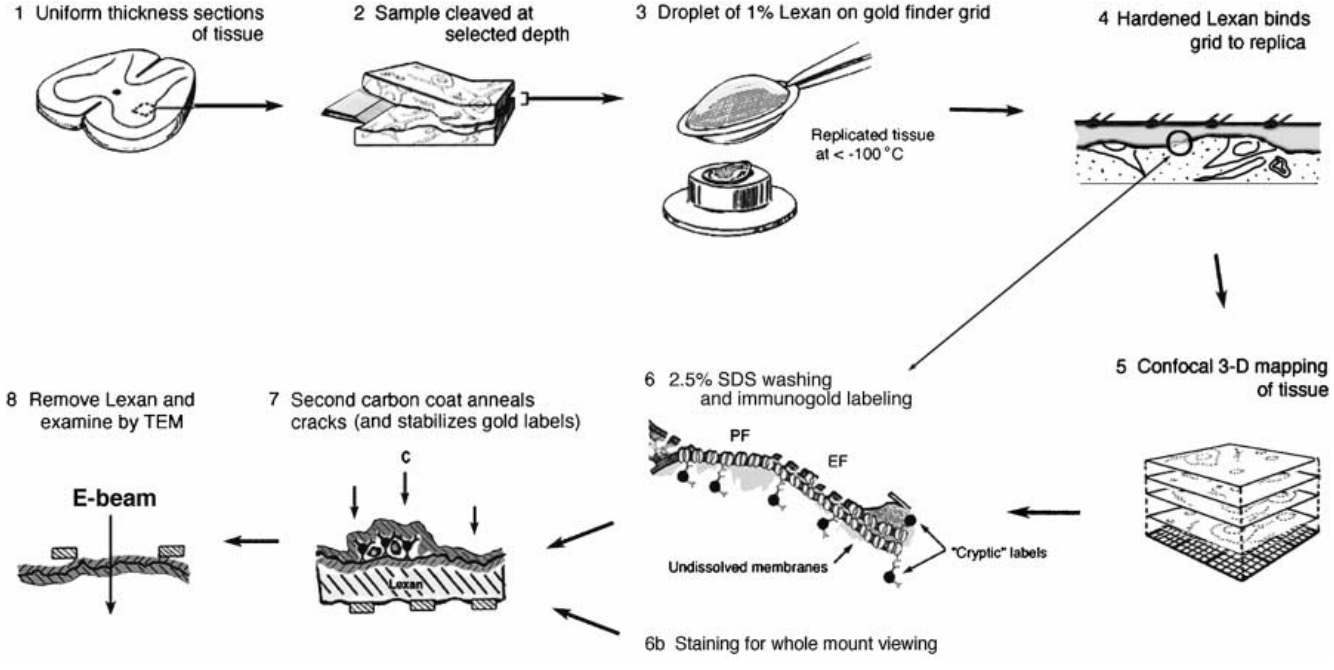

Fig. 1 *Steps 1–8.* Steps in the SDS-washed immunogold-labeled grid-mapped freeze-fracture technique. *Step 1* Uniformly thick sections were cut by using a vibratome. *Step 2* The samples were fractured at a pre-selected depth and shadowed with platinum and carbon. *Step 3* A gold index grid was bonded in Lexan plastic to the frozen tissue slice. *Step 4* The solvent (dichloroethane) was evaporated at –35°C, leaving the gold grid embedded in a thin film of plastic, which in turn, was bonded to the platinum/carbon layer on the replicated tissue. *Step 5* The grid-bonded tissue was thawed and photography-mapped by using confocal microscopy. *Step 6a* Washes over 24 h at 37°C in 2.5% SDS detergent left a thin film of biological material adsorbed to the replica. *Step 6b* To visualize the extent of undissolved material that remained after washing, some samples were contrasted with OsO_4, uranyl acetate, and lead citrate (*PF* P-face, *EF* E-face). In addition to membrane blebs, electron-dense staining revealed incompletely dissolved gap-junction plaques, which often extended 0.1–0.5 µm beneath the replica (designated "cryptic" labels). *Step 7* After air-drying, a second carbon coat was applied to the labeled "tissue-side" of the replica to stabilize the gold labels and to anneal cracks caused by thermal expansion as the replica was warmed from –180°C to +22°C. The Lexan backing film was removed by rinsing the sample in dichloroethane. *Step 8* The samples were examined at low to high magnification by transmission electron microscopy (*TEM*) and photographed as stereoscopic pairs

glycerol and frozen by contact with a –185°C "copper mirror" (Heuser et al. 1981; Phillips and Boyne 1984). Samples were freeze fractured and shadowed with 1 nm Pt/C and replicated with 5–10 nm carbon in a JEOL RFD9010 C freeze-fracture device (Fig. 1, Step 2). Replicated samples were removed via an airlock into a –180°C chamber containing dry nitrogen vapor. A gold "Finder Grid" was bonded to the frozen replicated tissue (Fig. 1, Steps 3, 4) by using 1.5–2% Lexan plastic (GE Plastics, Pittsfield, Mass.) dissolved in dichloroethane (Rash et al. 1995). After evaporation of the solvent at –35°C, the Lexan-stabilized samples were thawed, and the brain and spinal cord slices were photography-mapped by using a Molecular Dynamics Multiport 2001 inverted confocal microscope (Fig. 1, Step 5). To avoid both electrolytic alteration of platinum films and electrolytic deposition of colloidal gold or colloidal iron granules on the replicas (Rash et al. 1995), the grid-bonded replicas were manipulated in all aqueous solutions with ceramic (rather than metal) forceps.

Replica cleaning with SDS and immunogold labeling

To overcome surface "boundary layer" effects that interfere with washing the Lexan-bonded replicas, samples were washed at 35–60°C for 24–28 h with constant stirring in detergent solution (2.5% SDS, 10 mM TRIS HCl, pH 9). To investigate the effects of prolonged washing, some samples were washed for 48 h at 60°C. Replicas were washed for at least one additional hour after removal of all visible remnants of tissue and were then rinsed three times in SPB (pH 7.2–7.4, 5 min each; Fig. 1, Step 6a).

Before exposure to primary labels, detergent-washed samples were immersed for 1 h in "labeling-blocking buffer" (LBB; Dinchuk et al. 1987; Rash et al. 1990), consisting of 0.15 M SPB, plus 10% heat-inactivated goat serum and 0.5% teleost gelatin (Sigma). In some experiments, we employed 10% goat serum plus 0.01% bovine serum albumin in SPB, but this mixture proved slightly less effective than LBB. The proteins and peptide fragments in LBB are strongly adsorbed to the ultraclean Pt/C surfaces, thereby effectively blocking non-specific adsorption of primary and secondary labels (Dinchuk et al. 1987; Rash et al. 1990) and redeposition of dissolved membrane proteins.

Labeling methods

Lexan-stabilized samples were immersed for 1–1.5 h at 24°C in primary antibody solution (1 µg/ml stock solution mixed 1:100 with LBB; single antibodies or mixed primary antibodies from two or three species). Anti-connexin antibodies and immunogold reagents were from Chemicon (Temecula, Calif.). Antibodies to aquaporin-4 (AQP4)[1] were donated by Soren Nielsen, University of Aarhus, Aarhus, Denmark. Samples were rinsed (4×10 min each) in LBB and counter-labeled for 2 h with species-specific antibodies coupled to 10-nm, 20-nm, and/or 30-nm gold. Alternatively, some liver samples were counter-labeled with protein-A/10-nm gold (Chemicon). LBB was equally effective at blocking non-specific adsorption with IgG-gold or protein A-gold. Labeled replicas were rinsed in LBB (5×10 min each), twice in SPB, and three times in distilled water and air-dried, and a second "backing" carbon coat was applied (see below).

[1] The "aquaporins" are a large class of water channels, one or more of which are present in the plasma membranes of all organisms (King and Agre 1996). AQP4 is particularly abundant in the pia-glia limitans and in astrocyte endfeet surrounding capillaries (Nielsen et al. 1997) and has recently been demonastrated by direct immunogold labeling to be the primary protein in the "square arrays" present at the same sites (Rash et al. 1998). We now extend that report by providing detailed methods and procedures for SDS-washing and immunogold labeling

Labeling controls

In double-labeling experiments, each primary antibody label served as an internal "pre-immune" control for the other label. Additional replicas were incubated with SPB containing no primary antiserum or with antiserum to an absent antigen. For all connexin-labeling experiments on brain and spinal cord tissues, an additional slice of liver was labeled with the same reagents. Liver gap junctions provided a positive control for Cx32 labeling (Beyer et al. 1990; Sosinsky 1995) and a negative control for Cx43 labeling. Liver was also used as the primary tissue for analyzing the dynamics of SDS-washing and for identifying sources of false-positive and false-negative labeling.

Multiple contrasting methods

Conventional staining of replica "whole-mounts"

To analyze the SDS-solubilization process, additional replicas were SDS-washed and labeled as above, rinsed, fixed for 1 h in 2.5% glutaraldehyde, post-fixed with 1% osmium tetroxide for 1 h, stained for 30 min with 0.5% uranyl acetate in distilled water, counter-stained for 10 s with lead citrate, and air dried (Fig. 1, Step 6b). This heavy-metal staining procedure (Rash et al. 1970) revealed the extent of partially dissolved membrane debris that remained immediately after labeling.

Two-sided shadowing

As a second method for revealing the thickness of the undissolved material that remained adhering to the replica, several labeled replicas (including several stained whole-mounts) were returned to the freeze-fracture device and a second coat of platinum was deposited on the labeled tissue-side of the replica. Because the second platinum coat was deposited at room temperature, it was distinguished from the first platinum layer by its coarser platinum grains (Rash and Yasumura 1992).

Secondary carbon coat and removal of the Lexan film

All labeled replicas (including replica whole-mounts) were rinsed and air-dried, and a second "backing" coat of carbon was applied on the labeled "tissue-side" of the replica (Fig. 1, Step 7). The second carbon coat annealed cracks created by thermal and mechanical stresses in the Lexan-backed Pt/C replica (Rash et al. 1995) and prevented displacement of the replica and of the gold labels during subsequent removal of the Lexan support film. The Lexan support film was removed by immersing the grid in dichloroethane (6 changes in 1–1.5 h). All samples were air-dried.

Electron microscopy

By using a JEOL 2000 EX-II TEM, labeled replicas were photographed as stereoscopic pairs, with an 8° included angle between images (Fig. 1, Step 8). Stereoscopic viewing is essential for distinguishing specific labeling, which is always on the reverse (or tissue-side) of the replica, from non-specifically adsorbed gold beads, which are usually on the obverse side (i.e, the surface initially coated with Lexan).

To assist the viewer in interpreting the complex three-dimensional relationships (e.g., the "sidedness" of specific and non-specific labels and associated membrane debris), selected images are presented as stereoscopic "triplets." For the stereo triplets, the normal stereoscopic perspective (parallel viewing axis) is presented as the left two of the three images, and the *intaglio* perspective (or reverse stereo) is presented as the right two of the three images. "Crossed-eyes" viewing results in the reversal of the stereopsis from that described here. Viewing stereo triplets is often required to overcome false perceptions derived from conventional macro-

scopic vision, where three-dimensional superposition is always inferred when an opaque structure obscures an object that is at a greater distance from the viewer. In contrast, opaque structures in TEM images may occur above or below translucent objects, potentially causing the naive viewer to assume incorrect three-dimensional relationships.

Stability of immunoreagents

Immunogold reagents aggregate or clump during freezing and thawing of stock solutions. Clumped immunogold reagents cause the artifactual amplification of apparent labeling efficiency, because even a few antibody molecules projecting from a clump may be sufficient to bind the clump to the replicated target IMPs. However, the number of gold beads within the clump is independent of the number of replicated IMPs or pits. Consequently, for statistical purposes, only single gold beads separated by more than 30 nm were counted. Closely spaced "doublets" and "triplets" were counted as single labels. For labeled replicas in which large clumps were observed, the offending reagents were discarded, and the data were considered separately under "artifacts". To minimize clumping, immunogold reagents were stored at 4°C and discarded after 3 months.

Determination of labeling efficiency; positive identification of target IMP arrays

To determine labeling efficiency (LE; Rash et al. 1990), we calculated the ratio of the number of gold labels to the number of IMPs in the candidate structure (i.e., connexons in gap junctions or aggregate number of IMPs in recognizable square arrays). To determine the signal-to-noise ratio (S:N; Rash et al. 1990), we compared the number of gold labels per unit area within candidate structures (i.e., gap junctions and square arrays) with replicated non-array plasma membrane, cytoplasm, and extracellular space. Typically, S:N varied from 100:1 to 500:1. With a high S:N and the absence of clumping, each gold bead acts as an independently-targeted label. Thus, multiple labels restricted to an identifiable class of IMPs on an identifiable class of cells provides confidence for the positive identification of labeled structures.

Results

Labeling and LE in SDS-washed replicas

Liver as primary model system

Slices of liver were used to determine basic cleaning and labeling parameters in the Lexan-stabilized samples. In liver slices labeled with anti-Cx32 and protein-A/10-nm gold, gold beads were found in abundance only in direct association with gap junctions (Fig. 2). Gold beads were present at an LE of about 1 gold label per 100 connexons (LE=1:100 or 1%), equivalent to 110 gold beads per square micrometer of gap junction. Notably, both P- and

Fig. 2 Gap junctions in adult rat liver labeled with anti-Cx32 and counter-labeled with protein A/10-nm gold. A large gap junction (ca. 12 000 connexons) labeled with 114 gold beads (LE=1:105). Of nine gap junctions, eight are labeled (*black arrows* point to three examples of small gap junctions that are labeled). Two gold beads (*white arrows*) are present in areas normally occupied by gap junctions but are not associated with recognizable arrays of IMPs or pits. Both E- and P-faces are labeled at approximately the same labeling efficiency. Overall, the signal/noise ratio was S:N=500:1. ×63 000

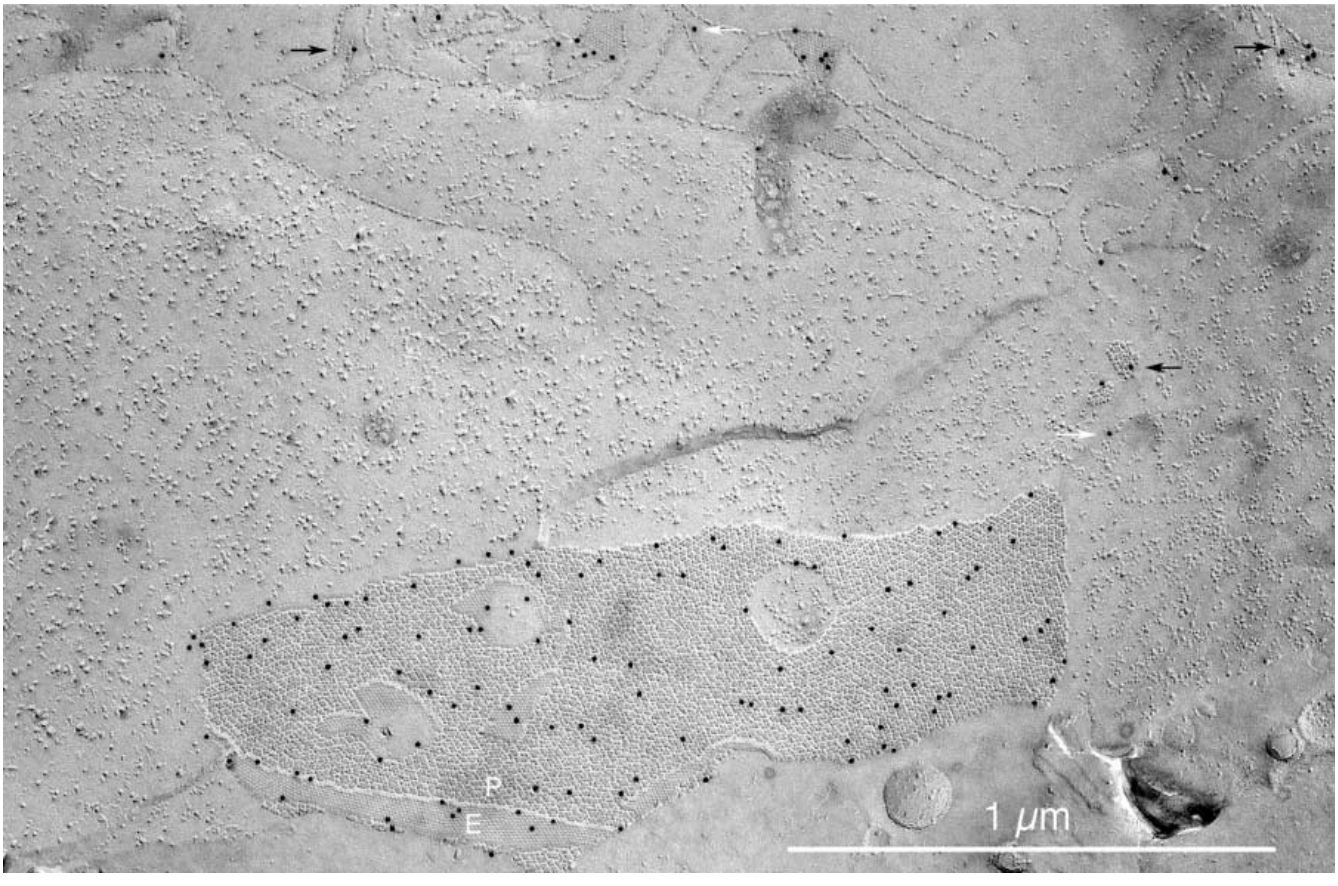

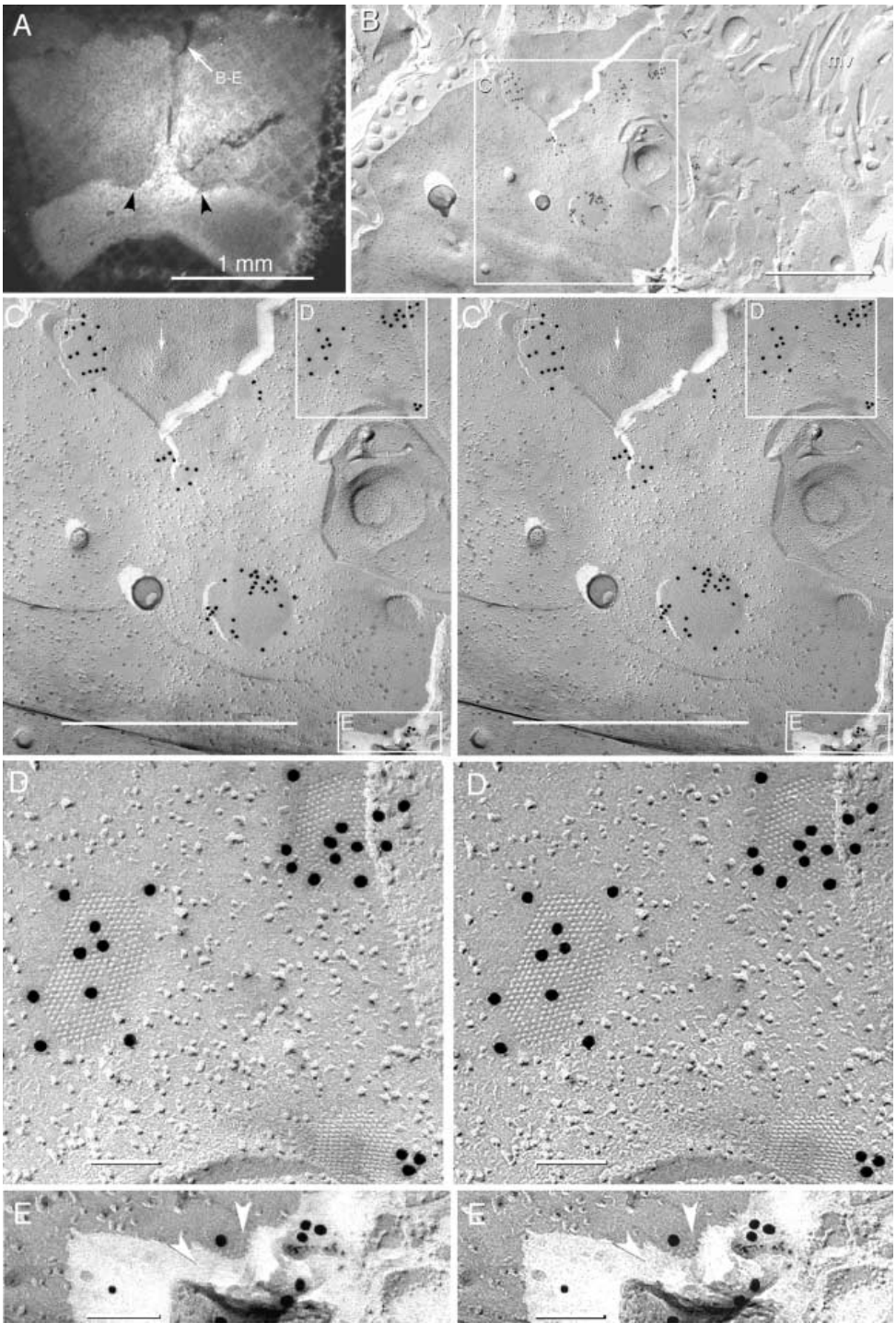

Fig. 3A–E Grid-mapped freeze-fracture replica from the suprachiasmatic nucleus (SCN) of adult rat brain. **A** Confocal image (inherent tissue fluorescence) of a cross section through the optic chiasm (*white band*) and SCN. The two shallow indentations in the optic nerve define the lower margins of the paired SCN (*arrowheads*). ×22. **B–E** These micrographs were obtained from a tissue slice at the point indicated by the *labeled arrow* in **A**. **B** Low-magnification image of ependymocytes that line the third ventricle of the brain. Microvilli (*mv*) mark the apical surface of ependymocytes. The inscribed area is shown at higher magnifications in **C–E**. ×16 000. **C** Eight of nine gap junctions in this area are labeled with anti-Cx43/20-nm gold. An unlabeled gap junction (*white arrow*) is seen in the P-face. Inscribed areas **D** and **E** are shown at higher magnification in succeeding images. ×35 000. *Bars* (**B, C**)*:* 1 µm. **D** Higher magnification image of three labeled gap-junction E-faces. Stereoscopic viewing reveals that all gold beads are beneath the replica, bound to connexons of the adjacent coupled cell. ×125 000. **E** Ependymocyte gap junction that was detected solely because it was immunogold labeled. Most of the gap junction is hidden in the platinum-free "shadow" cast by an adjacent ridge. However, the hexagonal array of E-face pits (*right arrowhead*) continues into and is faintly detectable in the electron-transparent carbon replica (*left arrowhead*). ×120 000. *Bars* (**D, E**) 0.1 µm

E-face images of gap junctions were labeled equally well (see below).

Non-junctional plasma membranes were essentially devoid of labels (0.1–1/µm^2), yielding an S:N of 100:1 to 500:1 (methods for distinguishing "signal" from "noise" are described below). At an LE of 1:100, small gap junctions typically were labeled with 1–5 gold granules (Fig. 2A, black arrows). However, a few of the smallest gap junctions were unlabeled, apparently reflecting the probabilistic nature of the immunogold labeling process. Overall, the washing, blocking, and labeling procedures on Lexan-stabilized replicas were sufficiently developed to permit application to complex tissues.

Cx43 in virtually all astrocyte and ependymocyte gap junctions

Freeze-fractured and replicated slices of rat brain and spinal cord were photographed by confocal light micros-

Fig. 4A, B A 10-µm² area containing astrocyte gap junctions labeled with anti-Cx43/20-nm gold. **A** Four labeled gap junctions (*1–4*) linking eight astrocyte processes. ×40 000. **B** Higher magnification stereoscopic image of gap junction *3* in **A**. Twenty-three gold beads are beneath approximately 600 connexons (LE=1:30; S:N=>2000/1). ×85 000. *Bar* (**B**) 0.1 µm

copy before SDS cleaning and immunogold labeling (Fig. 3A). By using the photomaps as guides, the ciliated and microvilli-rich ependymal cell layer was located quickly by electron microscopy (Fig. 3B-E). In the samples labeled for Cx43 (and AQP4, see below), 20-nm gold beads were present beneath the replicas of almost all gap junctions of identified ependymocytes (Fig. 3C-E) and astrocytes (Fig. 4A). The larger gap junctions of ependymocytes exhibited abundant labeling, with very few gold beads in non-junctional areas (LE=1:30). Of the nine small gap junctions illustrated in Fig. 3C, eight were labeled. Non-specific labeling was virtually non-existent (i.e., S:N=>500:1). Moreover, in such replicas with low background, clusters of 20-nm gold beads almost invariably delineated gap junctions, some of which would probably have gone undetected by conventional search strategies (Fig. 3F; see below).

Cx43-labeling was also found in the cytoplasmic side of most astrocyte gap junctions, including astrocyte-to-ependymocyte and astrocyte-to-astrocyte gap junctions (Fig. 4) and in the astrocyte cytoplasm of astrocyte-to-oligodendrocyte gap junctions. Cx43 labeling was not found within oligodendrocytes in their couplings with astrocytes (Rash et al. 1999). These observations con-

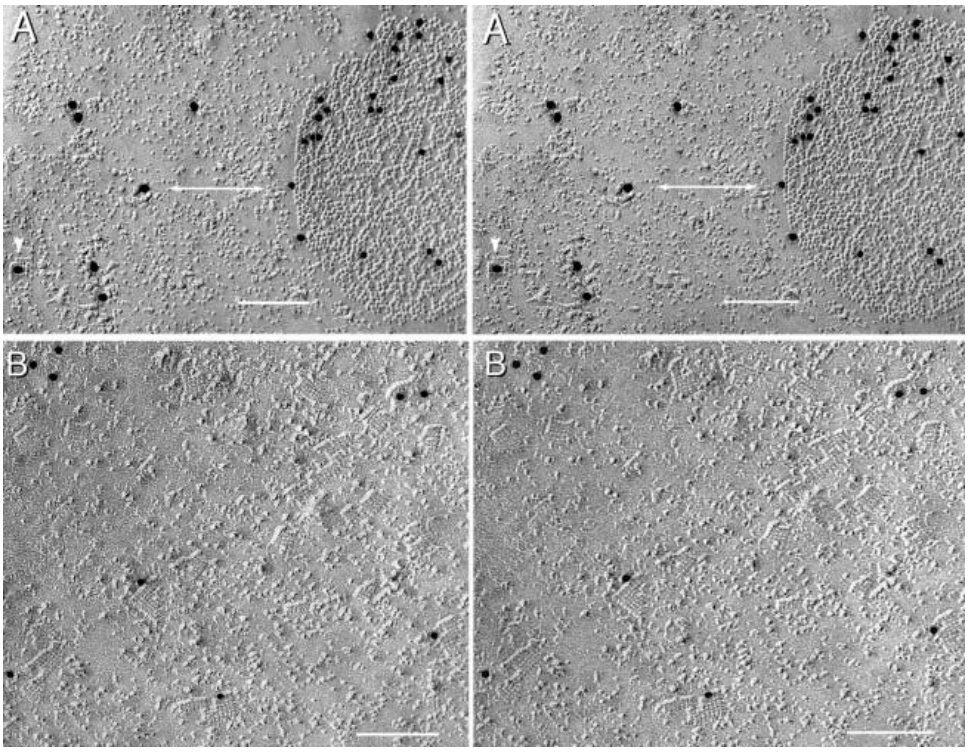

Fig. 5A, B Ependymocytes and astrocytes double-labeled for Cx43 and AQP4. **A** P-face of ependymocyte. In a reversal of our normal convention, the gap junction is labeled with anti-Cx43/10-nm gold, whereas the square arrays are labeled with anti–AQP4/20-nm gold (*arrowhead*). *Double-ended arrow* Two sizes of a gold particle. ×75 000. **B** Astrocyte square arrays labeled with anti-AQP4/10-nm gold. The smaller gold beads do not obscure as much detail as the larger beads used above. The overall labeling efficiency was 1:3 square arrays or 1:80 IMPs (for details of square array ultrastructure, see Rash et al. 1997, 1998). ×115 000. *Bars* 0.1 µm

firmed similar distributions of Cx43 seen in labeled thin sections (Nagy et al. 1997, 1998). Overall, immunogold tagging for Cx43 greatly simplified the search for ependymocyte and astrocyte gap junctions in all regions of brain and spinal cord, thereby allowing us to find large numbers of gap junctions for subsequent statistical analysis.

Simultaneous "double labeling"

The simultaneous application of two (or three) different species-specific antibodies to different membrane proteins, followed by species-specific immunogold labels of different diameters allows the simultaneous identification and mapping of two or more proteins. For example, simultaneous labeling with monoclonal mouse antibodies to Cx43 (with 10-nm gold) and polyclonal rabbit antibodies to AQP4 (with 20-nm gold) revealed Cx43 in ependymocyte gap junctions and AQP4 in the nearby square arrays (Fig. 5A). Reversal of secondary labels resulted in 10-nm gold on square arrays (Fig. 5B). Thus, double-labeling allows the simultaneous demonstration of two independent proteins in different IMP arrays in histologically mapped cells. Moreover, in double-labeling experiments, the absence of binding of one of the two labels may be concluded to arise either from the absence of one antigen or from a defective immunoreagent, and not from the lack of penetration of one of the two labels. On the other hand, the absence of both labels may indicate that SDS detergent has removed essentially all proteins from the replica film (see below). Finally, simultaneous double-labeling allows the qualitative comparison of the relative LEs of two labels.

Specific labeling

To identify sources and rates of non-specific labeling, all replicas were photographed and examined stereoscopically. Gold beads found in direct association with gap junctions were defined as specific labeling when they were: (1**)** present as "singlets," (2**)** located on the tissue-side of the replica, (3**)** located within 20 nm of identifiable P-face IMPs or E-face pits of gap junctions (Figs. 2–4), and (4**)** present in at least 100-fold excess over beads attributed to "non-specific labeling" (note: labeling apparently associated with E-face pits is observed only in membranes with paired coupled structures, such as gap junctions).

Non-specific adsorption

To identify and quantify sources of non-specific adsorption of labels, some samples were inadequately blocked and incompletely rinsed after labeling. Stereoscopic viewing allowed gold beads resulting from specific labeling to be identified among the high non-specific "background" (Fig. 6A; replica shadowed on both sides). On the tissue side of the replica, the highest density of gold beads was within the perimeter of the gap junctions, thereby identifying those as "specific" labels. In contrast, all of the abundant gold beads on the obverse surface of

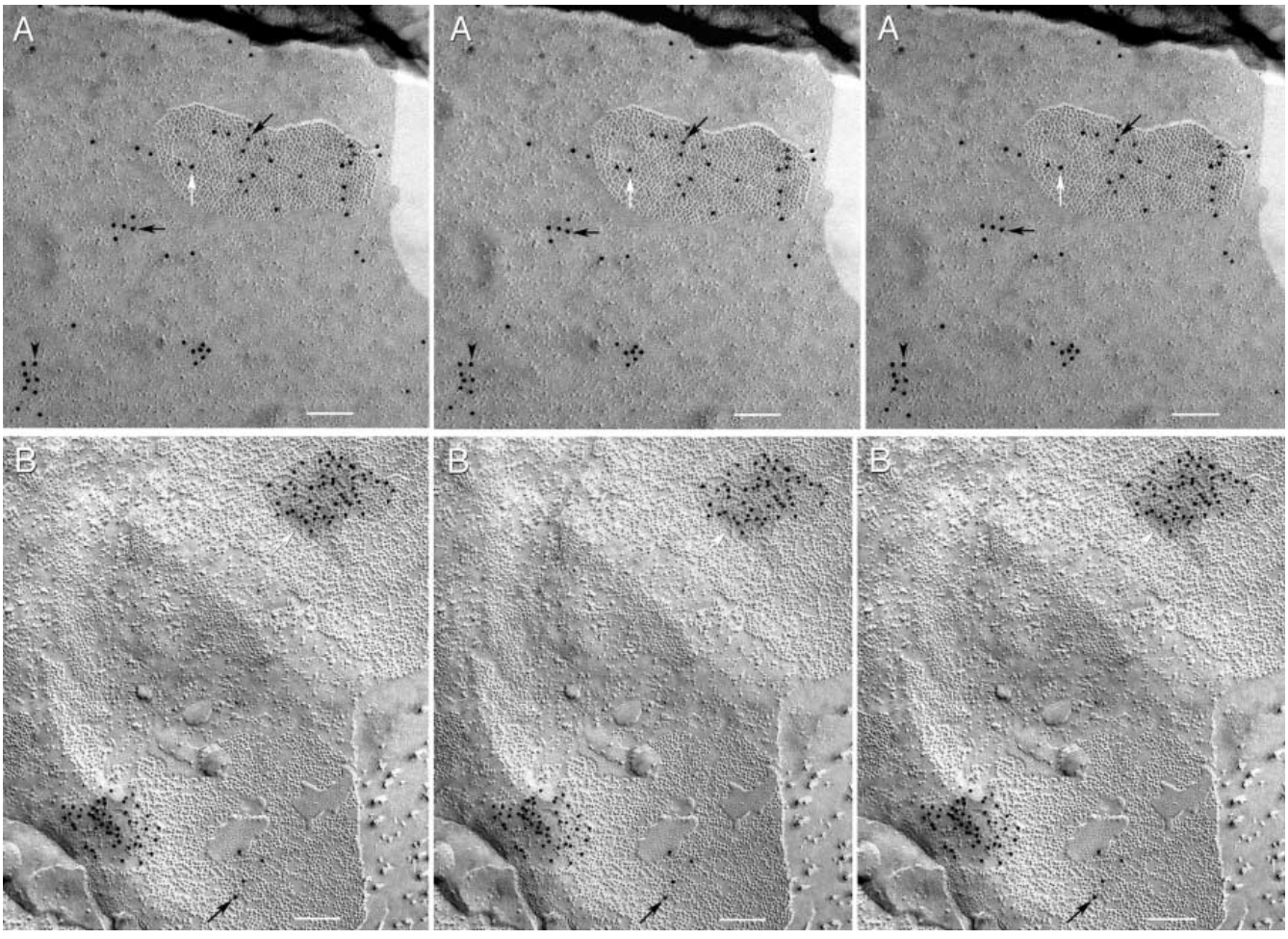

Fig. 6A, B Artifacts of immunogold labeling: non-specific adsorption and "clumping" of immunogold reagents. **A** Gap junction in rat liver labeled with anti-Cx32/20-nm gold and inadequately rinsed. Specific labeling is present beneath the replicated gap junction (*white arrow*). However, the high level of non-specific labeling is reflected in the large number of gold beads on the upper (formerly Lexan-coated) surface of the replica (*black arrows*). The high level of non-specific labeling is also indicated by gold beads beneath the replica but is not associated with gap junctions (*black arrowhead*). ×60 000. **B** Ependymocyte gap junction labeled with two clumps (one at *white arrow*) and three single gold beads (*black arrow*). Typically, clumps are confined and delineated within a volume of increased electron opacity (*white arrow*) and hence do not resemble regions of closely spaced singlet labels. Note that the lower clump only partially overlaps the gap junction. The overall low level of labeling results from the more than 1000-fold reduction of singlet gold labels because of clumping. ×60 000. *Bars* 0.1 μm

the replica were attributed to "non-specific adsorption". This included one gold bead on the upper surface of the replica but within the perimeter of the gap junction (Fig. 6A, arrowheads). Finally, several clusters of gold beads were found on the tissue-side of the replica, but outside the perimeter of gap junctions. These, too, were identified as non-specific labeling attributable to inadequate washing. From these and similar experiments under a variety of labeling conditions, we determined that more than 90% of non-specific labeling occurred on the upper (obverse) surface of the replica.

Artifacts and anomalies of freeze-fracture immunogold labeling

Clumped secondary labels

"Clumping" of immunogold secondary antibodies causes artifactual amplification of labeling, whether in freeze fracture (Fig. 6B), conventional TEM, or LM immunocytochemistry. However, in freeze-fracture replicas, clumping of immunogold is easily identified, because clumps of densely packed gold beads are delineated within a well-defined matrix of increased electron-density (Fig. 6B, white arrow). Frequently, clumps only partially overlapped the target arrays (Fig. 6B), thereby revealing that not all of the gold beads within the clumps were bound to target proteins. Nevertheless, clumps inappropriately appear to amplify the "signal" because hundreds or even thousands of gold beads in a clump may become associated with the appropriate targets, but only a few of the beads may be bound to individual connexons. Therefore, each clump is considered to represent only one, or at most, a few "hits." In the example provided, only six hits would have been counted: four as

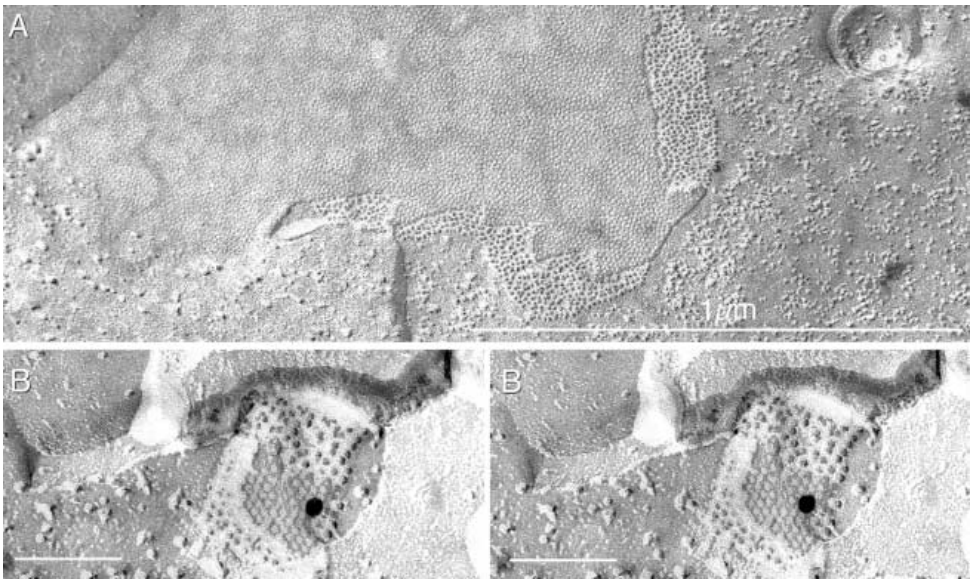

Fig. 7A, B Artifacts of immunogold labeling: false-negative and false-positive labeling. **A** Rat liver gap junction that was washed excessively (48 h at 60°C) prior to immunogold labeling with anti-Cx32/20-nm gold. No gold beads were present on any of the gap junctions found in this sample. ×70 000. **B** Astrocyte gap junction false-positively labeled with anti-Cx43/20-nm gold. The single gold bead is above the replica and above a thin layer of residual Lexan, where no immunological determinants are present. Without stereoscopic imaging, this image would probably have been attributed to specific labeling. In samples with low background, false-positive labeling is very rare. ×150 000. *Bar* (**B**) 0.1 µm

singlets and two as clumps. When clumping occurred, however, it also resulted in significantly reduced "signal" from singlet labels, because most of the gold beads had been removed from solution by aggregation into the clumps. Thus, in labeled replicas, as in thin sections, evidence of significant clumping of reagents requires that the samples should not be used for statistical analysis.

False-negative labeling

False-negative labeling may occur when samples are washed excessively in SDS. After washing for 24 h at 37°C (and at 60°C ; not shown), strong labeling was seen (Fig. 2), whereas after washing for 48 h at 60°C, all labeling was eliminated (Fig. 7A). Thus, the occurrence of false negatives is of concern, because it implies that the precise conditions and durations of SDS-washing may be critical in obtaining standardized conditions, particularly when attempting semi-quantitative analysis or comparative analysis of various classes of proteins. False-negative labeling also implies that the adsorption of proteins to the Pt/C replica is completely reversible under prolonged washing conditions.

False-positive labeling

In contrast to false negatives, false-positive labeling was rare in LBB-protected replicas. When antibodies to an absent antigen were used, false-positive labeling on the tissue side of any specific target array was extremely rare. Nevertheless, one form of false-positive labeling occurred when gold beads were found associated with candidate structures, but the beads lay on the obverse surface, where no immunospecific binding is possible (Fig. 7B**)**. Without stereoscopic viewing, such obverse-side labeling would probably be misinterpreted as target-specific labeling.

"Cryptic" labeling

"Cryptic" labeling is defined here as the specific labeling of unreplicated but inferentially detected target-rich membrane fragments. Based on this definition, the following three groups can be distinguished.

E-face labeling: a form of "cryptic" labeling

Any label associated with E–face pits represented a form of "cryptic" labeling, because the labeled proteins were in the gap-junction plaque of the contiguous cell and were neither exposed by fracturing nor replicated by Pt/C. We were intrigued by the finding that E-face images of gap junctions were equally-well or better labeled than the nearby P-face particles (Figs. 2, 3C, 4, 10A). Fujimoto (1995) noticed a similar labeling of E-face pits but accounted for the apparent discrepancy by suggesting that carbon atoms that had been deposited at the bottoms of the E-face pits in one cell became directly adsorbed to the underlying connexin molecules of the contiguous cell. However, we note that. in contrast to P-face IMPs, which are completely enveloped in carbon, the area of contact of the carbon film with the connexin proteins at the bottom of the E-face pits is minimal. Thus, we suspect that an alternative mechanism is responsible for stabilizing the proteins of the underlying unreplicated membrane bilayer. One possibility is that substantial material remained undissolved beneath the replica/tissue interface but was not detected because of its low electron opacity. Another possibility is that the proteins in the underlying gap-junction plaque were solubilized by SDS but always drifted toward and were adsorbed by the platinum film precisely within the perimeter of the original gap-junction E-face. Evidence for the first possibility (i.e., undissolved membrane components) is presented below.

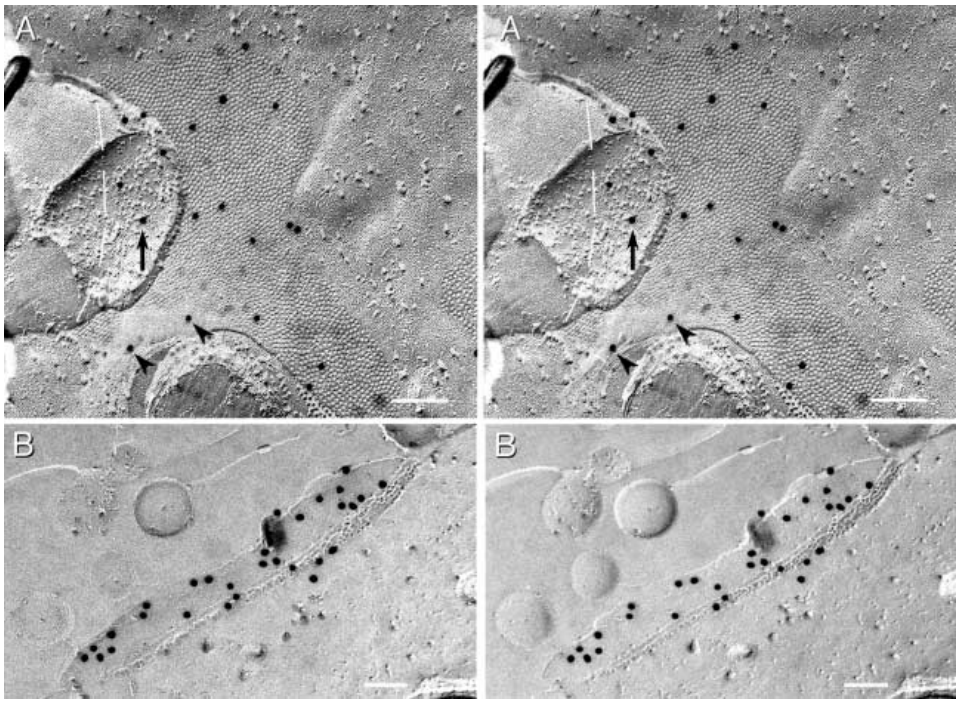

Fig. 8A, B Forms of "cryptic" labeling. **A** Anti-Cx32-labeled gap junction in rat liver. The fracture plane was diverted from within the gap junction to an overlying cytoplasmic membrane. A *dashed line* is drawn connecting the margins of the gap junction. Gold beads are present beneath the cytoplasmic membrane (*arrow*) and beneath areas fractured and replicated with carbon only (*arrowheads*). ×76 000. **B** Cross-fractured gap junction between astrocyte processes. Anti-Cx43 labeling abruptly ends at the lateral margin of the area of close membrane apposition but continues beneath the replica in the direction projected by the plane of the extant gap junction as it existed prior to SDS digestion. Note that air-drying of labeled replicas causes the gold beads to collapse against the replica. ×60 000. *Bars* 0.1 µm

"Cryptic" labeling beneath the cytoplasmic matrix

"Cryptic" labeling also occurred where the fracture plane was diverted from a gap-junction E-face into the overlying cytoplasm (Figs. 8A–B). Labeling frequently occurred up to 0.5 µm beyond the replicated gap-junction E-face (Fig. 8B, arrows), usually within the predicted perimeter of the gap junction where it extended beneath the cytoplasm. The predicted perimeter of each gap junction was defined by drawing a line connecting the margins of the gap junction at the sites where the fracture plane was diverted into the cytoplasm (Fig. 8A, dashed line). Again, from the presence of "cryptic" label, we suspected that undissolved membrane fragments remained associated with the replicated gap junctions.

"Cryptic" labeling of cross-fractured gap junctions

Occasionally, gold beads were seen to be aligned along one or both sides of cross-fractured plasma membranes, precisely where the extracellular space was narrow. In many images tilted perpendicularly to the areas of close membrane apposition (Fig. 8B), a few P-face IMPs or E-face pits in distinctive hexagonal arrays could be observed, confirming that the areas of close apposition represented cross-fractured gap junctions. However, the number of gold beads was far in excess of the number predicted based on the number of replicated IMPs or pits, suggesting that approximately 0.1–0.3 µm of paired undissolved membrane remained attached beneath the replica.

Stained whole-mounts of labeled replicas

To test the hypothesis whether only a single monolayer (i.e., half membrane) of adsorbed proteins remained attached to the replica film (Fujimoto 1995) or whether attached undissolved membrane remnants represented the primary source of both direct labeling and "cryptic" labeling (this report), several SDS-washed labeled replicas were fixed, stained, and examined as "whole-mounts" (Fig. 9). Two forms of undissolved or partially-dissolved membrane debris were revealed. Electron-translucent "blebs" ranging from 50 nm to 200 nm in diameter were detected beneath and attached to freeze-fractured membranes, primarily in areas containing few IMPs. These membrane blebs created during SDS-washing closely resembled blebs formed during protease disruption of membranes (Klymkovsky et al. 1980).

In other stained whole-mount preparations (Fig. 9B), a continuous, approximately 20-nm-thick layer of semi-opaque material was observed within the perimeter of the replicated gap-junction E-face pits and P-face IMPs (Fig. 9B, arrowheads). In contrast, the areas surrounding the gap junction exhibited distinctive blebs that presumably represented the dissolving osmiophilic lipid matrix of the membranes. Almost all gold labels were confined to the electron-dense plaques but occasionally were present in blebs at the edges of gap junctions (arrow). Thus, we conclude: (1**)** that densely packed proteins (e.g., gap junctions and square arrays) are more resistant to SDS washing than lipid-rich membrane regions, and (2**)** that at least some of the SDS-resistant proteins retain immunogenicity. In addition, heavy-metal staining revealed the extent of undissolved membrane debris and thereby permitted the analysis of washing dynamics. Finally,

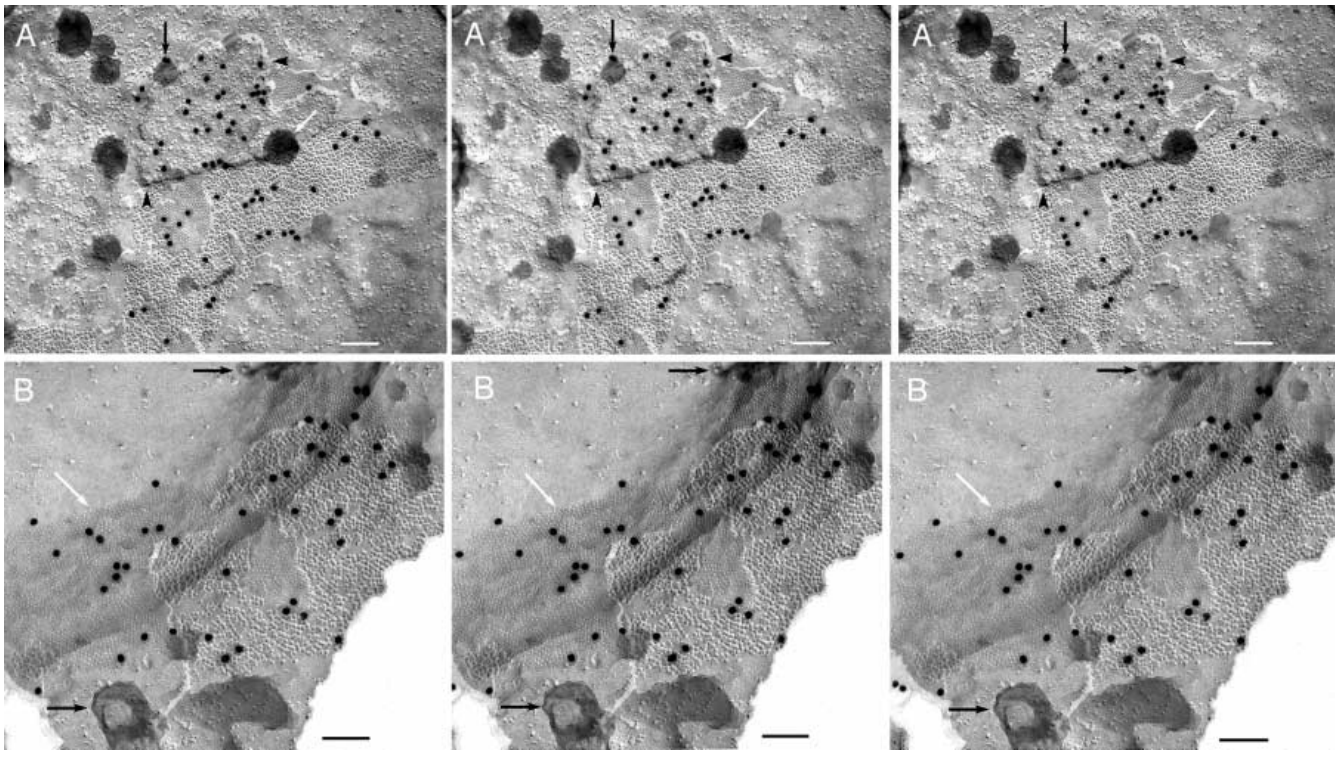

Fig. 9A, B Stained "whole-mount" preparations. **A** Liver gap junction labeled with anti-Cx32/20-nm gold. Electron-dense membrane blebs in various states of dissolution are visible beneath the replica. One bleb at the margin of the gap junction contains a single gold bead (*black arrow*). Most blebs were fixed while detaching from areas of lipid-rich non-gap-junctional plasma membrane. The central bleb (*white arrow*) was in the process of detaching from a flattened subsurface cistern (subjunctional endoplasmic reticulum). The presence of the underlying gap junction was inferred based on its interrupted perimeter (*arrowheads*) and on the presence of "cryptic" labels. ×50 000. **B** At high tilt (images made at 36° and 44° tilt), the margin of a protein-rich gap junction plaque is evident (*white arrow*). Although most of the lipid-rich extra-junctional plasma membrane has been dissolved or is present as membrane blebs (*black arrows*), the protein-rich gap junction appears to have been more resistant to the SDS-washing procedure. Gold beads are present only within the margin of the gap junction. ×70 000. Bars 0.1 µm

these images showing a moderately low LE (1:100) despite the presence of relatively intact gap-junction plaques reveal that only a small portion of the remaining connexons are labeled. We conclude that further improvements in replica cleaning and labeling may yet be obtained.

Relative adsorptivity of carbon and platinum surfaces

Fujimoto (1995) hypothesized that membrane integral proteins that had been exposed and directly coated with carbon under ultra-clean high-vacuum conditions would be strongly adsorbed to the replica film. To test this hypothesis, we examined areas in several replicas where carbon but not platinum was deposited. In small areas where structures with high topographic relief blocked the deposition of platinum (Fig. 10A) and in larger areas where the local shadowing angle resulted in an absence of platinum (Fig. 11A), we observed plaques of gold beads approximating the density and distribution seen in nearby platinum-replicated gap junctions. Moreover, we were astonished at the level of detail resolvable in optimally underfocussed images of these carbon-replicated junctions (Fig. 10C). In digitally processed, high-contrast, high-density images, the presence of hexagonally arranged P-face IMPs and E-face pits was revealed, as were finer details within individual connexons that normally are obscured by the electron-dense platinum coat. When samples were tilted so that the central axis of each connexon was parallel to the electron beam, carbon-replicated connexons were revealed in "negative contrast" (Fig. 10C). In many connexons, the six peripheral subunits and the central canal (Caspar et al. 1977) were clearly delineated (Fig. 10 C, arrow).

In gap junctions that were replicated with carbon only (Fig. 11B), hexagonal arrays of E-face pits were detected as faint impressions in the carbon films. These otherwise invisible gap-junction E-face plaques had been detected solely because of the attached gold labels. More importantly, the high level of labeling of carbon-replicated gap junctions clearly documented that the gap-junction proteins were equally well or better adsorbed to pure carbon films than to conventional Pt/C films. Thus, the carbon component of freeze-fracture replica films appears to be sufficient to account for all adsorptivity of the Pt/C replicas (Dinchuk et al. 1987; Andersson Forsman and Pinto da Silva 1988; Rash et al. 1990; Fujimoto 1995). Because of technical limitations in depositing pure platinum, we have as yet been unable to determine the role of

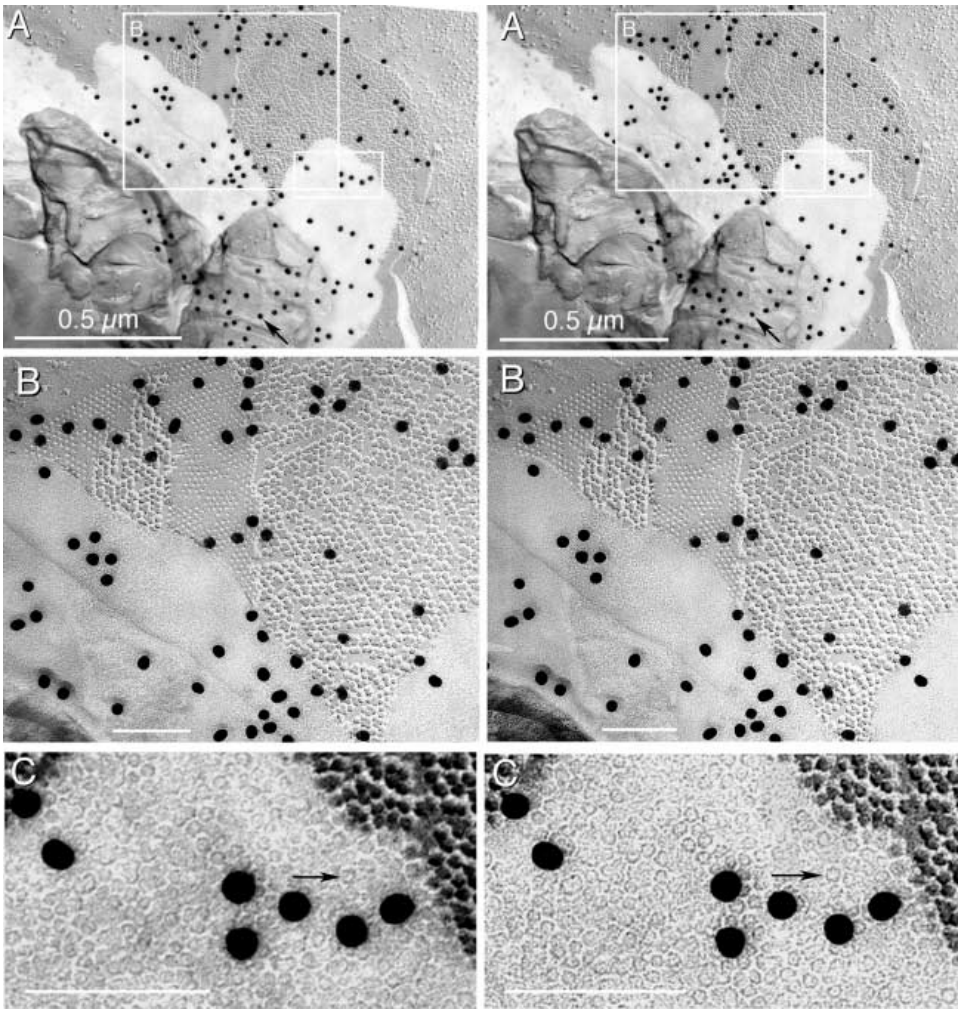

Fig. 10A–C Specific immunogold labeling of carbon-replicated connexons. **A** Obliquely shadowed debris prevented deposition of platinum over portions of a large gap junction between ependymocytes. The anti-Cx43/20-nm gold label continues uninterrupted beneath the replicated debris. Note that rotary carbon coating (with continuous tilting) penetrated beneath the debris (*black arrow*), thereby preserving and faintly delineating the P-face IMPs and E-face pits (**B, C**). ×42 000. **B, C** Successively higher magnifications of the central region in **A**. Both E- and P-faces are labeled. In high-magnification stereoscopic images, the 2- to 3-nm-thick carbon coat applied to the vertical sides of the connexons is seen to delineate in negative contrast the central channel and the six connexin subunits of many connexons (**C** *black arrow*). **B** ×92 000, **C** ×230 000. *Bars* (**B, C**) 0.1 μm

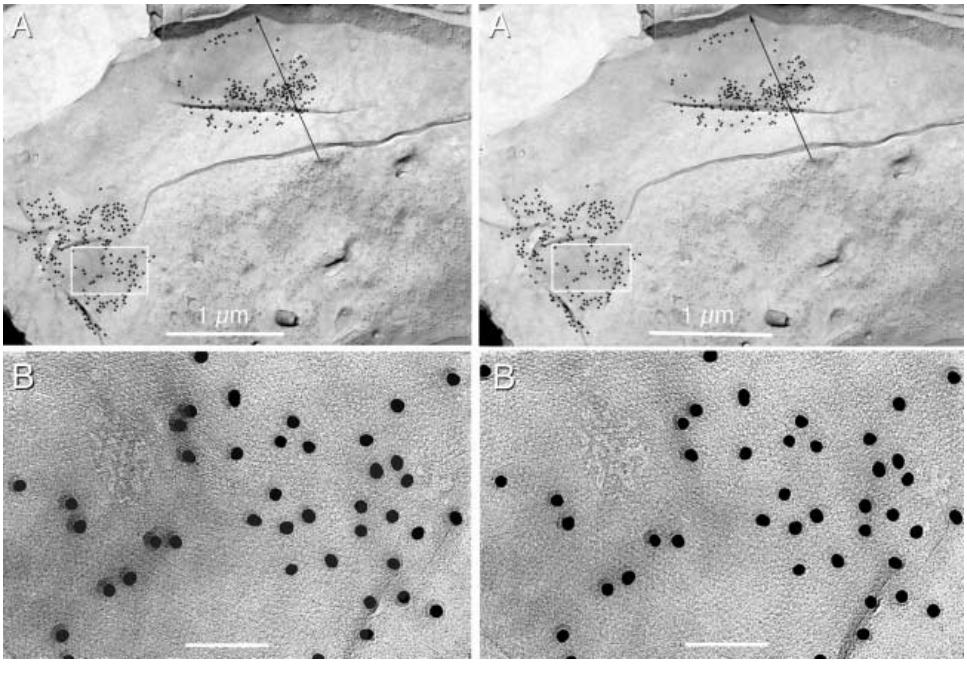

Fig. 11. A Two patches of anti-Cx43 immunogold labeling on an area of replica that was not shadowed with platinum because of local three-dimensional relief. The *long black arrow* traces the angle and path of platinum deposition and delineates a structure casting a distinct shadow contour. Gold beads are present in distributions characteristic of immunogold-labeled gap junctions, as is shown in a higher magnification view of the inscribed area (**B**). ×16 000. **B** By using digital contrast enhancement, gold beads were confirmed as being present beneath the characteristic hexagonal arrays of gap-junction E-face pits. Immunogold labeling in the carbon-replicated areas was approximately two-fold higher than immunogold labeling of platinum-shadowed gap junctions elsewhere in the same replica. ×110 000. *Bar* (**B**) 0.1 μm

platinum in increasing or decreasing protein adsorption to the replica.

Discussion

We have used sequential freeze-fracture replication and Lexan-stabilization (Rash et al. 1995, 1996), in concert with confocal histological mapping, detergent-cleaning, and immunogold labeling (SDS-FRL; Fujimoto 1995, 1997) to demonstrate the direct immunocytochemical identification and subcellular localization of multiple membrane proteins in complex tissue. We have correlated the labeled IMP aggregates with specific cells and tissue layers previously photographed by confocal microscopy. We have also investigated the relative contributions of platinum and carbon to the stabilization of membrane constituents at the replica/tissue interface, and the dynamics and extent of membrane solubilization by SDS detergent.

Although we have been able to label and identify clustered IMPs, we note that whether dispersed membrane proteins (e.g., neurotransmitter receptors, metabolite pumps, or ion channels) remain adsorbed to the replica in sufficient numbers to be identified by similar immunogold labeling techniques has not been determined. Thus, in order to extend these methods to the identification of other classes of membrane proteins, it is appropriate to begin investigations of each component of the replica-stabilization, SDS-washing, and immunogold-labeling procedures.

Factors affecting the retention of clustered and dispersed IMPs

Finely divided platinum and activated charcoal have long been used as organic catalysts, adsorbants, and purifying agents, in part because both provide highly adsorptive surfaces onto which many organic compounds bind strongly. Potentially, freeze-fracture replicas combine the adsorptive properties of both platinum and carbon in the replica film. Under the high-vacuum conditions of freeze-fracture, platinum and carbon atoms are condensed directly from the vapor phase onto newly created, ultraclean fracture faces. This strong adsorptivity results in high levels of non-specific binding of immunological labels in all areas of the replica (Dinchuk et al. 1987; Rash et al. 1990). In replicas of cell suspensions washed of all serum proteins (which otherwise act as endogenous "blocking" agents; Dinchuk et al. 1987; Rash et al. 1990), "non-specific labeling" is often more than 3,000 gold beads/μm^2. Consequently, we have developed LLBs that minimize the non-specific adsorption of primary and secondary immunogold labels based on the mass occupation of available adsorption sites by non-immunogenic "blocking" molecules (Dinchuk et al. 1987; Rash et al. 1990). With the application of LBB prior to primary labeling, non-specific binding can be reduced to less than $1/\mu m^2$ (often to less than $0.1/\mu m^2$), which is 3–5 orders of magnitude lower than the concentration of connexins in gap junctions, and 2–3 orders of magnitude lower than the density of specific labeling at gap junctions (this report). With current immunogold reagents, the resulting S:N ratios of 100:1 to 500:1 allow great confidence in the designation of labeled IMP arrays.

Platinum vs carbon as the primary adsorptive substance

In 1995, Fujimoto hypothesized that the carbon atoms of freeze-fracture replicas are so strongly adsorbed to replicated membrane macromolecules that membrane proteins and lipids would not be removed by washing in strong detergents. This conjecture appears to be at least partially correct. Another possibility is that the hydrophobic carbon film stabilizes the hydrophobic surface of split membranes. Our examination of areas replicated with carbon (i.e., no platinum) has confirmed Fujimoto's suggestion that immunogold labeling does not require the presence of platinum for stabilizing gap-junction proteins. Moreover, regions of immunogold-labeled freeze-fracture replicas in areas devoid of platinum repeatedly show equal or greater labeling than regions consisting of mixed Pt/C. Thus, we conclude that the strong stabilizing properties of vapor-deposited carbon, in combination with "boundary layer effects" and mass interaction, are sufficient to account for the observed differential retention of replicated clusters of membrane proteins following vigorous washing in SDS detergent.

Differential solubilization of membrane lipids and proteins

In this study, we have used electron-dense staining and double-shadowed labeled-replica whole-mounts to examine the structural sequence of tissue solubilization during SDS washing. Osmiophilic (and therefore presumably lipid-rich) membrane blebs have been found beneath areas of the plasma membrane that contain dispersed IMPs. Moreover, stained whole-mount preparations have revealed that residual material of variable thickness provides the basis for all labeling by SDS-FRL, including both "specific" labeling and "cryptic" labeling.

In contrast to IMP-deficient areas of the plasma membrane, IMP-rich areas (e.g., gap junctions, square arrays) show few blebs and appear relatively intact. These observations suggest that SDS detergent preferentially solubilizes lipid-rich membrane regions, and that areas containing SDS-resistant clustered proteins are differentially retained for immunogold labeling. However, even gap junction and square array proteins are not completely resistant to SDS solubilization. After 48 h of SDS washing at 60°C, no connexins are detectable by immunogold labeling. These observations suggest that further refinements in detergent washing may yet be obtained.

Under appropriate conditions, it may become possible to identify dispersed membrane proteins by direct immunogold labeling (J. E. Rash, T. Yasumura, and S. Nielsen, unpublished).

Labeling artifacts and anomalies

In this study, we have identified four primary types of labeling artifacts: "false negatives," "false positives," "non-specific adsorption," and labeling of "cryptic" (or unreplicated) antigenic sites. "Cryptic" labeling is abundant in samples with high levels of specific labeling, reflecting primarily the presence of unreplicated but incompletely dissolved membrane fragments. False-negative labeling is attributed primarily to excessive washing, whereas "false-positive" labeling has been traced to the use of ineffective blocking buffers, to incomplete rinsing, or to the redeposition of labels displaced during removal of the Lexan support film. In this regard, we have shown that more than 90% of non-specific adsorption of label occurs on the obverse side of the replica, where immunological binding to in situ tissue antigens is not possible. Consequently, we suggest that when labels are sparse, confirmation of labeling requires the stereoscopic demonstration of multiple dispersed labeling on the tissue-side of the replica and in direct association with an identifiable class of IMPs.

Gold beads serve as "flags" to increase the probability of finding rare structures

Many gap junctions (and other target structures) are overlooked during conventional searches, because of (1) an inappropriate local shadowing angle and loss of specimen contrast, (2) the small size of the target structure, or (3) by being obscured or hidden by other structures. Because of their high intrinsic opacity and high visual contrast, multiple large gold beads (i.e., 20 or 30 nm) are readily discerned and, consequently, greatly increase the probability of finding labeled structures. For example, during our examination of gap junctions replicated with carbon only, we have found gap junctions in areas in which previously we would not have searched (Figs. 3E, 11A). Thus, immunogold labeling may prove particularly beneficial when attempting to identify rare membrane proteins.

Unresolved problems

Inherent variabilities in SDS washing and in Pt/C or carbon stabilization of adsorbed proteins currently preclude reliable quantitative analysis of membrane proteins. Nevertheless, labeling densities range from 1 gold bead per 100 connexons to as high as 1 gold bead per 8 connexons in some replicas. Above this density, it may become difficult to distinguish between clumped labels and closely packed single labels. Nevertheless, low to moderately efficient labeling is sufficient for determining the presence of a particular protein within an IMP array and for semi-quantitative analysis.

The current low LE of SDS-washed replicas may be the result of: (1**)** damage to antibody binding sites by bombardment with white-hot platinum and carbon during the replication process (Bachmann et al. 1969), (2**)** excessive washing and removal of most protein from the replicated membrane, (3**)** a rearrangement of membrane lipids and proteins during SDS cleaning, with subsequent masking of or damage to antibody binding sites, or (4**)** as yet unrecognized artifacts of the grid-mapped freeze-fracture replication process. Regardless of these unresolved issues, freeze-fracture immunogold labeling now seems to be a highly sensitive and highly accurate tool for the direct identification and subcellular mapping of clustered membrane proteins. Further refinements in washing and labeling methods may make this technique useful for both qualitative and quantitative analysis of membrane protein arrays in diverse tissues.

Acknowledgments We thank Dr. Soren Nielsen for the gift of antibodies to AQP4.

References

Andersson Forsman C, Pinto da Silva P (1988) Fracture-flip: new, high resolution images of cell surfaces after stabilization of freeze-fractured membranes. J.Cell Sci 90:531–541

Bachmann L, Aberman R, Zingsheim HP (1969) Hochauflösende Gefrierätzung. Histochemie 20:133–142

Beyer EC, Paul DL, Goodenough DA (1990) Connexin family of gap junction proteins. J Membr Biol 166:187–194

Branton D (1971) Freeze-etching studies of membrane structure. Philos Trans R Soc Lond Biol 261:133–138

Caspar DLD, Goodenough DA, Makowski L, Phillips WC (1977) Gap junction structure. I. Correlated electron microscopy and X-ray diffraction. J Cell Biol 74:605–628

Dinchuk JE, Johnson TJA, Rash JE (1987) Postreplication labeling of E-leaflet molecules: membrane immunoglobulins localized in sectioned labeled replicas examined by TEM and HVEM. J Electron Microsc Tech 7:1–16

Fisher KA, Branton D (1976) Freeze-fracture autoradiography: feasibility. J Cell Biol 70:453–458

Fujimoto K (1995) Freeze-fracture replica electron microscopy combined with SDS digestion for cytochemical labeling of integral membrane proteins. Application to the immunogold labeling of intercellular junctional complexes. J Cell Sci 108:3443–3449

Fujimoto K (1997) SDS-digested freeze-fracture replica labeling electron microscopy to study the two-dimensional distribution of integral membrane proteins and phospholipids in biomembranes: practical procedure, interpretation and application. Histochem Cell Biol 107:87–96

Heuser JE, Reese TS, Dennis MJ, Jan Y, Jan L, Evans L (1981) Synaptic vesicle exocytosis captured by quick freezing and correlated with quantal transmitter release. J.Cell Biol. 275: 275–300

Hudson CS, Rash JE, Shinowara N (1981) Freeze-fracture and freeze-etch methods. In: Johnson JE (ed) Current trends in morphological techniques, vol II. CRC Press, Boca Raton, pp 183–217

King LS, Agre P (1996) Pathophysiology of the aquaporin water channels. Annu Rev Physiol 58:619–648

Klymkovsky MW, Heuser JE, Stroud RM (1980) Protease effects on the structure of acetylcholine receptor membranes from *Torpedo californica*. J Cell Biol 85:823–838

Nagy JI, Ochalski PAY, Li J, Hertzberg EL (1997) Evidence for co-localization of another connexin with connexin-43 at astrocytic gap junctions in rat brain. Neuroscience 78:533–548

Nagy JI, Patel D, Occhalski PAY, Stelmack GL (1998) Connexin30 in rodent, cat and human brain: selective expression in gray matter astrocytes, co-localization with connexin43 at gap junctions and late developmental appearance. Neuroscience 88:447–468

Nielsen S, Nagelhus EA, Amiry-Moghaddam M, Bourque C, Agre P, Ottersen OP (1997) Specialized membrane domains for water transport in glial cells: high-resolution immunogold cytochemistry of aquaporin-4 in rat brain. J Neurosci 17:171–180

Phillips TE, Boyne AF (1984) Liquid nitrogen-based quick freezing: experiments with bounce-free delivery of cholinergic nerve terminals to a metal surface. J Electron Microsc Tech 1:9–29

Pinto da Silva P, Parkinson C, Dwyer N (1981a) Freeze-fracture cytochemistry: thin sections of cells and tissues after labeling of fracture faces. J Histochem Cytochem 8:917–928

Pinto da Silva P, Torrisi MR, Kachar B (1981b) Freeze-fracture cytochemistry: localization of wheat-germ agglutinin and concanavalin A binding sites on freeze-fractured pancreatic cells. J Cell Biol 91:361–372

Rash JE, Yasumura T (1992) Improved structural detail in freeze-fracture replicas: high-angle shadowing of gap junctions cooled below –170°C and protected by liquid nitrogen-cooled shrouds. J Electron Microsc Tech 20:187–204

Rash JE, Biesele JJ, Gey GO (1970) Three classes of filaments in cardiac differentiation. J Ultrastruct Res 33:408–435

Rash JE, Hudson CS, Graham WF (1978) Ultrastructure of acetylcholine receptors at the mammalian neuromuscular junction. In: Straub RW, Bolis L (eds) Cell membrane receptors for drugs and hormones: a multidisciplinary approach. Raven, New York, pp 47–68

Rash JE, Johnson TJA, Hudson CS, Copio DS, Graham WF, Eldefrawi ME, Giddings FD (1980) Identification of intramembrane particles by pre- and post-fracture labelling techniques: a progress report. Ann Proc Electron Microsc Soc Am 38: 692–695

Rash JE, Hudson CS, Mayer RF, Graham WF (1981) Freeze-fracture, labelled-replica, and electrophysiological studies of junctional fold destruction in myasthenia gravis and experimental autoimmune myasthenia gravis. Ann N Y Acad Sci 377:38–60

Rash JE, Johnson TJA, Dinchuk JE, Duch DS, Levinson SR(1990) Labeling intramembrane particles in freeze-fracture replicas. In: Hui SW (ed) Freeze-fracture studies of membranes. CRC Press, Boca Raton, pp 41–59

Rash JE, Dillman RK, Morita M, Whalen LR, Guthrie PB, Fay-Guthrie D, Wheeler DW (1995) Grid-mapped freeze fracture: correlative confocal laser scanning microscopy and freeze-fracture electron microscopy of preselected cells in tissue slices. In: Severs NJ, Shotton DM (eds) Rapid freezing, freeze fracture, and deep etching. Wiley-Liss, New York, pp 127–150

Rash JE, Dillman RK, Bilhartz BL, Duffy HS, Whalen LR, Yasumura T (1996) Mixed synapses discovered and mapped throughout mammalian spinal cord. Proc Natl Acad Sci USA 93:4235–4239

Rash JE, Duffy HS, Dudek FE, Bilhartz BL, Whalen LR, Yasumura T (1997) Grid-mapped freeze-fracture analysis of gap junctions in gray and white matter of adult rat central nervous system, with evidence for a “panglial syncytium” that is not coupled to neurons. J Comp Neurol 388:265–292

Rash JE, Yasumura T, Hudson CS, Agre P, Nielsen S (1998) Direct immunogold labeling of aquaporin-4 in “square arrays” of astrocyte and ependymocyte plasma membranes in rat brain and spinal cord. Proc Natl Acad Sci USA 95:11981–11986

Rash JE, Yasumura T, Dudek FE (1999) Ultrastructure, histological distribution, and freeze-fracture immunocytochemistry of gap junctions in rat brain and spinal cord. Cell Biol Int (in press)

Severs NJ (1989) Freeze-fracture cytochemistry: review of methods. J Electron Microsc Tech 13:175–203

Singer SJ, Nicolson GL (1972) The fluid mosaic model of the structure of cell membranes. Science 75:720–731

Sosinsky G (1995) Mixing of connexins in gap junction membrane channels. Proc Natl Acad Sci USA 92:9210–9214